

Transceiver 4-leg birdcage for high field MRI: knee imaging

S.E. Solis^{a,b}, G. Cuellar^a, R.L. Wang^b, D. Tomasi^a, A.O. Rodriguez^{a,*}

^aCentro de Investigación en Instrumentation e Imagenología Médica, Universidad Autónoma Metropolitana Iztapalapa, Mexico, D.F. 09340, Mexico.

^bMedical Department, Brookhaven National Laboratory, Upton, NY, 11973, USA.

Recibido el 18 de octubre de 2007; aceptado el 11 de abril de 2008

The radiofrequency coil is a crucial component of the magnetic resonance imaging scanners, so that a solid knowledge on the design and physical characteristics is important for those interested in its development. A birdcage coil with a 10 cm radius and 4 legs (length = 12cm), and a separation between the copper strips of 4 cm, was developed for magnetic resonance imaging (MRI) of the human knee and tuned at the resonance frequency of protons at 4 Tesla (170.3 MHz). MR images were acquired with this coil in phantoms and in the knee of a healthy volunteer using a standard spin echo sequence. The phantom images demonstrated the high uniformity of the radiofrequency field with high signal-to-noise ratio, a characteristic of all birdcage RF coils. The *in vivo* knee images demonstrated that this birdcage geometry is ideal for knee imaging, promising MR images of the knee with higher spatial resolution at 4 Tesla. This work also demonstrates that volume coils are a good choice for high-field MRI applications.

Keywords: knee MRI; birdcage coil; electromagnetic simulation; high field

Las antenas de radio frecuencia son una parte crucial para los sistemas de imagenología por resonancia magnética (IRM), por lo que la adquisición de conocimientos sólidos en el diseño y características es importante para aquellos interesados en su desarrollo. Construimos una antena del tipo jaula para IRM de rodilla humana. El prototipo está compuesto de un diámetro de 10 cm, 4 elementos cuya longitud es de 12 cm y tienen una separación de 4 cm entre cada elemento y opera a la frecuencia de 170.3 MHz (4 Tesla). La viabilidad de la antena se probó con la adquisición de imágenes por resonancia magnética y de una rodilla sana, junto con secuencias estándar de tipo eco espín. Las imágenes mostraron alta calidad del cociente señal ruido y uniformidad del campo. Las imágenes adquiridas de la rodilla demostraron que la geometría tipo jaula es ideal para obtener imágenes de rodilla con alto cociente señal ruido en altos campos magnéticos. Este trabajo de investigación muestra que las antenas de volumen son una buena opción para aplicaciones de IRM de altos campos.

Descriptores: IRM de rodilla; antena de jaula de perico; simulación electromagnética; alto campo.

PACS: 87.57.-s; 87.62.+n; 87.61.-c; 84.32

1. Introduction

The radio frequency (RF) coil is one of the most important factors influencing the signal-to-noise ratio (SNR) in magnetic resonance imaging (MRI) experiments. The RF coil is a resonant device used for transmitting and receiving electromagnetic energy at the resonance frequency of a given nucleus. RF coils must have a high-quality factor (Q) to generate images with a high signal-to-noise ratio (SNR) and produce a highly homogeneous RF field in the imaging region.

In MRI, the RF coils can be classified as either volume or surface coils. While volume coils surround a substantial portion of the body, surface coils cover only a small fraction of the surface of the imaging voxel. The most popular volume coil is the birdcage coil due to its better field uniformity and its high Q-value, but it suffers from relatively low SNR [1].

The principal aim of this work was to develop a birdcage coil for applications to high-field MRI. By doing so, we intend to show some practical and theoretical aspects of this type of coil to serve as a guide for others interested in developing RF coils. *In vivo* and *in vitro* coil testing was performed with a 4T whole-body MR imager. Phantom and knee images were acquired to demonstrate its viability to generate high-quality images with standard spin-echo sequences at high-field MRI. Uniformity results computed from phantom images showed that this coil design is able to generate high-

quality phantom images with standard echo spin sequences. Knee magnetic resonance images of a healthy male volunteer were also acquired and showed that the combination of MRI and the popular birdcage resonator is a good choice for high-field MRI applications.

1.1. Birdcage coils

The birdcage coil is probably the most popular coil choice for MRI since it introduces high radio frequency magnetic field homogeneity that guarantees a broad field of vision with an acceptable SNR. Another important feature is the ability to produce a circularly polarized field by means of quadrature excitation that increases SNR by a factor of $\sqrt{2}$ [2].

The birdcage resonator is a rolled-up ladder network comprising inductive strips and distributed capacitors. It can be considered a parallel transmission line [3] where the current flows along the ladder. If the current in the coil legs is of the form: $I = I_0 \sin(\omega t + \phi')$, then the field produced in the imaging region is extremely uniform, and rotates its direction with angular velocity ω . There is a progressive phase change dependent on frequency. The ladder forms a closed loop with a phase change of 360° at which the resonant frequency occurs. This circuit is essentially a lumped element balance delay line joined onto itself. It can also be regarded as an N segment low-pass filter. There is also a high-pass version

of the birdcage resonator in which the capacitors are evenly spaced around both end rings and the straight segments between the end rings are purely inductive. The high symmetry of the resonator facilitates the use of quadrature excitation and reception. Figure 1 shows schematics of the two different types of birdcage resonators and their equivalent circuit.

1.2. Quadrature detection

One consideration of widespread importance in an RF coil is the issue of quadrature drive. This refers to the ability of a set of coils to generate or detect the circularly polarised field. A field of this kind can be considered to comprise two fields each half of the value of the original field value, rotating in opposite sense. These types of fields are necessary to flip off the magnetisation from its position of thermal equilibrium in the Z direction down onto the XY plane. Figure 2b and 2c show an illustration for the quadrature layout and the coax-

ial cable position in the coil resonator. The birdcage four-fold symmetry generates a fundamental homogeneous mode, which is doubly degenerate. The two modes, corresponding to surface current densities proportional to $\sin(\omega t + \phi')$ and $\cos(\omega t + \phi')$, are geometrically and electrically orthogonal. Both modes are excited simultaneously but with a relative phase shift of 90° to produce a rotating B1 field. A great deal of effort has been dedicated to studying the electrical characteristics of the popular birdcage coil for the last 10 years by a number of researchers [4-11].

TABLE I.

	Number of coil legs		
Simulation parameters	4	6	8
Mesh element number	3256	3548	3918
Degrees of freedom	6713	7351	8149
Solution time [s]	0.265	0.281	0.375

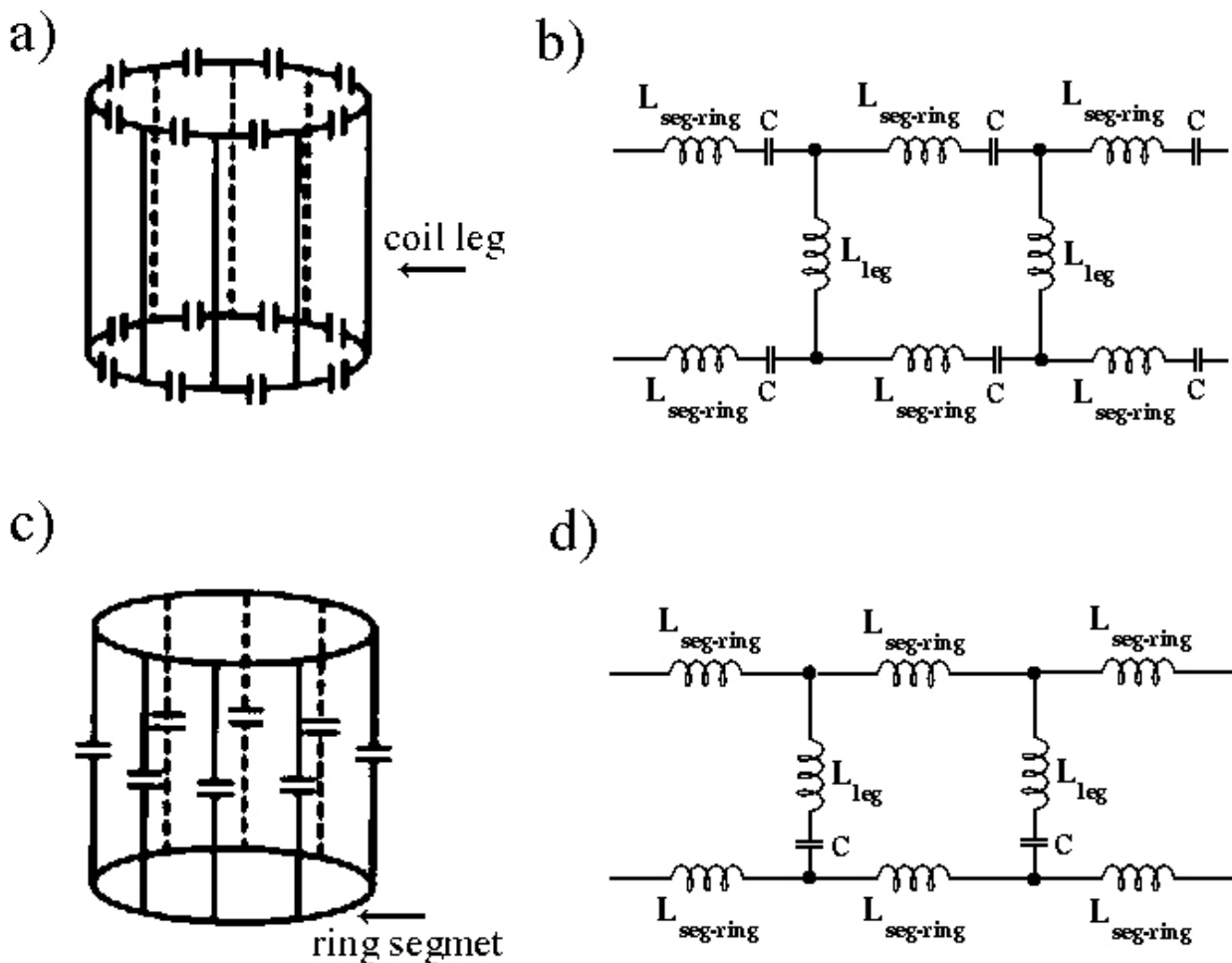


FIGURE 1. Schematic of high-pass birdcage coil (a) and its lumped element equivalent circuits (b). Schematic of low-pass birdcage and its equivalent circuit (d). L1 represents the inductance of the individual segments of the end rings, and L2 is the inductance of the straight legs of the coil.

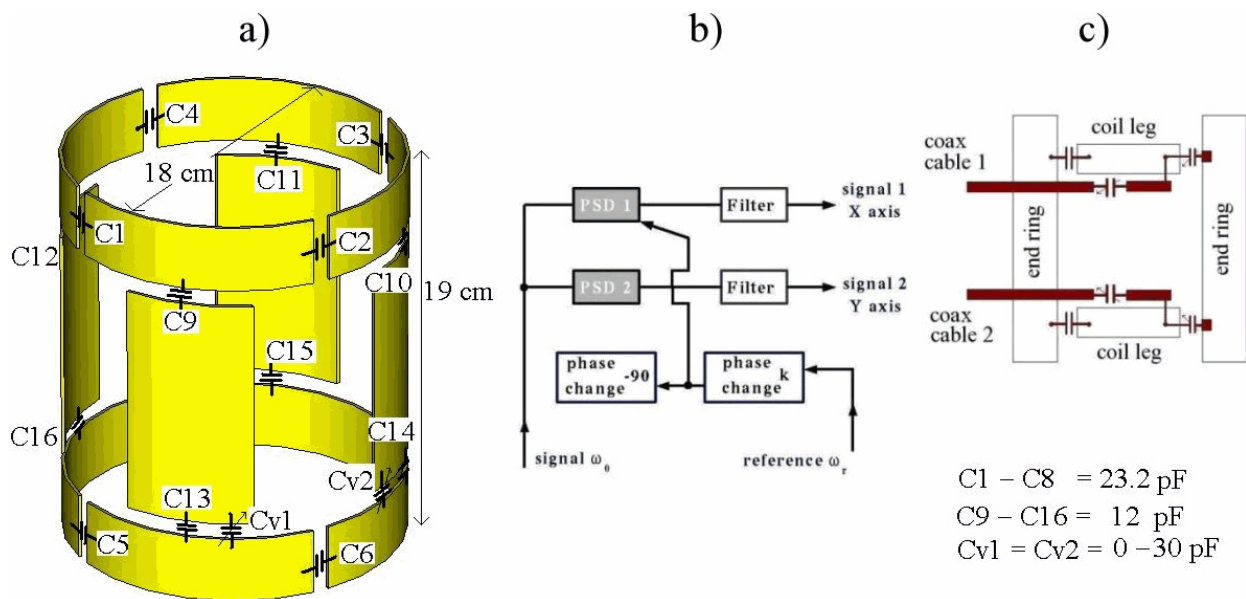


FIGURE 2. a) Schematic diagram of a transceiver band-pass birdcage coil indicating components. It can be advantageous to use more than one capacitor on each leg and end plate segment to avoid wavelength effects on long, unbroken conductive segments at high frequencies. b) A block diagram of a scheme for quadrature detection phase-sensitive detection (PSD). The reference phase may be adjusted as desired, before the reference is split into two, one of its branches having a phase shift of 90° . High-frequency components are removed by filtering the two products, and the two quadrature signals can be ready for digital processing and displaying. c) Localization of coaxial cables for the quadrature transmission/reception and electronics components.

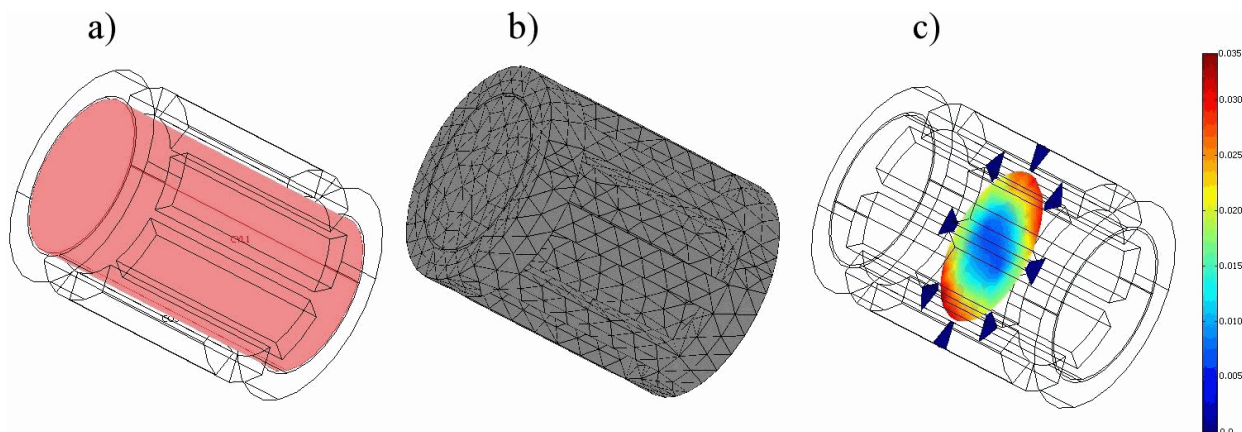


FIGURE 3. a) FEMLAB diagram of the 4-leg coil with phantom for B1 numerical simulations, b) simulation mesh with the number of elements indicated in Table I, and c) simulations were performed at the midsection of the resonator coil as illustrated.

2. Method

2.1. Simulation of RF coil field

The finite element method package FEMLAB (COMSOL, Burlington, MA, USA) was used to calculate the radiofrequency field B1 produced by the birdcage due to its ability to model complex geometric structures with acceptable accuracy. All numerical computations were carried out in a standard Intel PC running Windows OS. The simulation parameters are summarized in Table I. Figure 3 shows the schematics of the birdcage coil and the corresponding FEM mesh and the midsection where all simulations were carried out. The magnetic field B1 produced by the birdcage coil was numerically simulated for different numbers of legs.

2.2. Coil Design and Construction

A birdcage coil was built in our laboratory as a pass-band circuit as shown in Fig. 2a. The coil prototype dimensions were based on an optimised birdcage coil as reported in [12]. It was 12 cm long with an inner diameter of 18 cm. The 4-leg birdcage coil was assembled with 20 mm wide copper for the legs and the end rings had a 180 mm diameter. Two 50Ω-coaxial cables were attached to the coil to transmit/receive the MR signal to the scanner in quadrature mode. Non-magnetic capacitors of 23.2 pF and 12 pF were equally distributed around the coil as schematically shown in Fig. 2a. Each coil channel was matched to 50Ω and tuned to 170.29 MHz with two non-magnetic 30-pF variable capacitors. The separation

between the copper strips (4 cm) was large enough to ensure that the mutual inductance was negligible.

2.3. Measurement of coil quality factor (Q)

The Q-factors for the prototype coil with quarter-wavelength coaxial cable at the input of the coil (see Fig. 2c) for both channels was measured as the ratio of the resonant frequency to the frequency bandwidth (Δf) at 3 dB of S11 using a network analyzer (Model 4396A, Hewlett Packard, Agilent Technologies, CA). The frequency bandwidth was measured at 3 dB below the reference level, see Fig. 4a). The coil was tuned to 170.3 MHz and matched to 50 Ω . This measurement was done for the loaded (with a saline phantom at the coil center; see Fig. 4b) and the unloaded (without phantom) cases. The quality factor was measured for both channels to determine the performance of the coil, as mentioned above. The Q-factors for the unloaded and loaded cases were 20.035 and 18.888, respectively. No significant differences in the quality factor were observed for channels 0 and 90°.

2.4. Imaging experiments

All MR imaging experiments were performed in a 4-Tesla (170 MHz proton resonance frequency) whole-body superconducting magnet interfaced with an INOVA console (Varian, Inc, Palo Alto, CA, The USA) and SONATA (Siemens Medical Solutions, Malvern, PA, The USA) gradients. A spherical phantom (radius = 9 cm) was filled with distilled water containing creatine (methyl guanidine-acetic acid; 50 mM), N-acetyl aspartate (12.5 mM), choline (3.0 mM),

myo-inositol (7.5 mM), and glutamate (12.5 mM) and used for the imaging experiments. Fig. 4c shows a photo of the specially-built phantom. A healthy male provided written consent for his involvement in this study in accordance with the local Institutional Review Board. The volunteer's right leg was placed in the centre of the birdcage prototype, which was placed in the isocentre of the MRI scanner, as demonstrated in Fig. 5. The Phantom images were acquired with the coil prototype and spin-echo sequences (TR/TE=3000/130 ms, FOV=16×16 cm, slice thickness=5 mm, NEX=1, transversal matrix size=256×256, and sagittal matrix size=128×256). Scilab programs (V. 4.1, Consortium Scilab, INRIA, ENPC, France) were specially-written to compute the B1 uniformity profile of the birdcage resonator.

2.5. Three-dimensional image reconstruction

Bi-dimensional images are limited to appreciate both morphology and function of tissues and organs. The construction of a three-dimensional model of an organ and tissue from several two-dimensional images of it can provide us with the means to study them more efficiently. Knee images were converted to the ANALYZE™ format [13] and the image database consisted of at least two files: a) an image file, and b) a header file. The files have the same name being distinguished by the extensions .img for the image file and .hdr for the header file. Thus, for the image database heart, they are the UNIX files heart.img and heart.hdr. The ANALYZE™ programs all refer to this pair of files as a single entity named heart. The format of the image file is a very simple one of

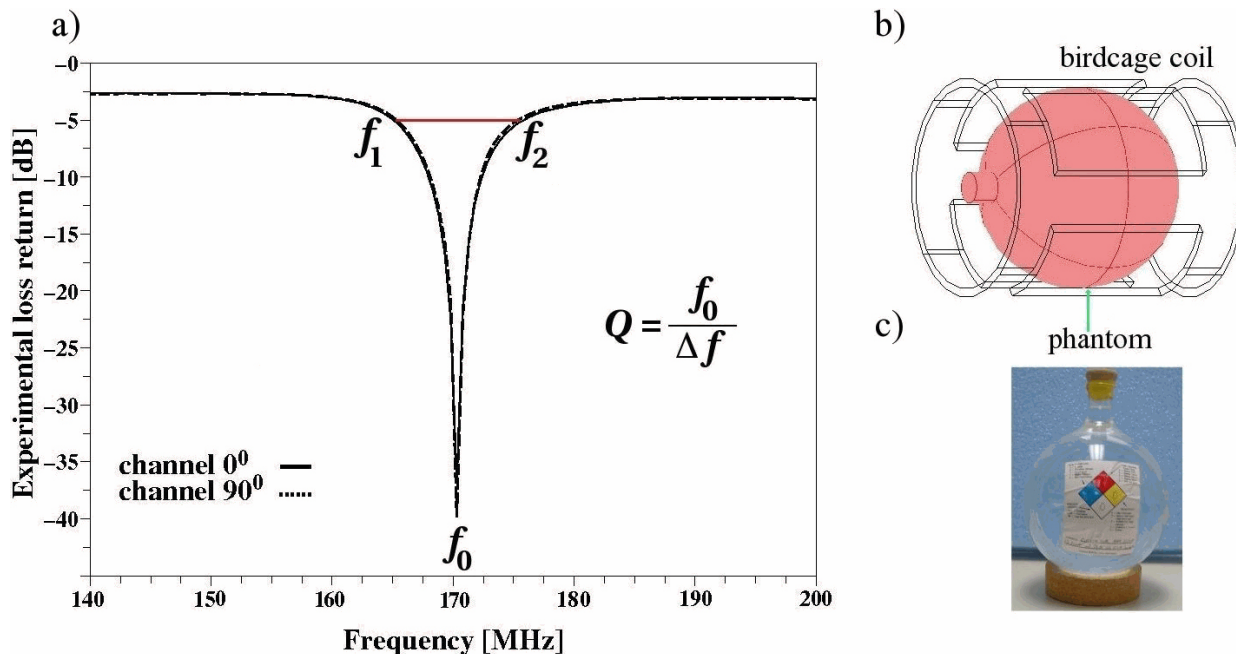


FIGURE 4. a) Experimental loss returns for both channels: 0° degrees and 90° as determined by the quadrature drive of Fig. 2b. b) Experimental setup to generate images with spherical phantom and the 4-leg birdcage resonator. c) Photograph of specially-built phantom for *in vitro* imaging.

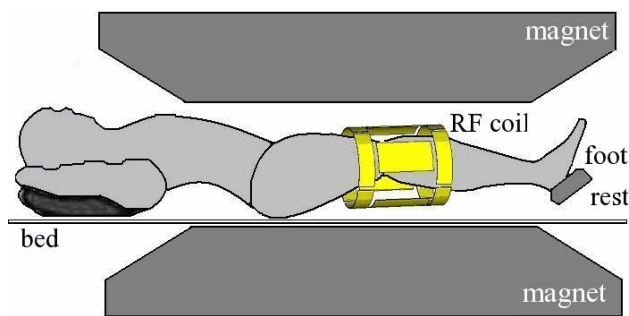


FIGURE 5. Experimental setup used to acquire knee imaging showing the volunteer position and location of the birdcage coil.

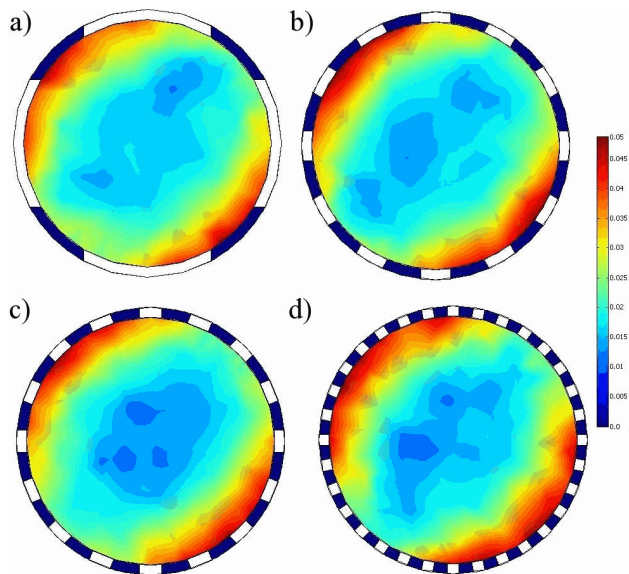


FIGURE 6. These two-dimensional plots illustrate simulations of the B1 field of our birdcage coil varying the number of legs at the resonant frequency of 170 MHz: a) 4 legs, b) 4 legs, c) 6 legs, and d) 8 legs. The white rectangular areas around the figure perimeter represent the coil legs.

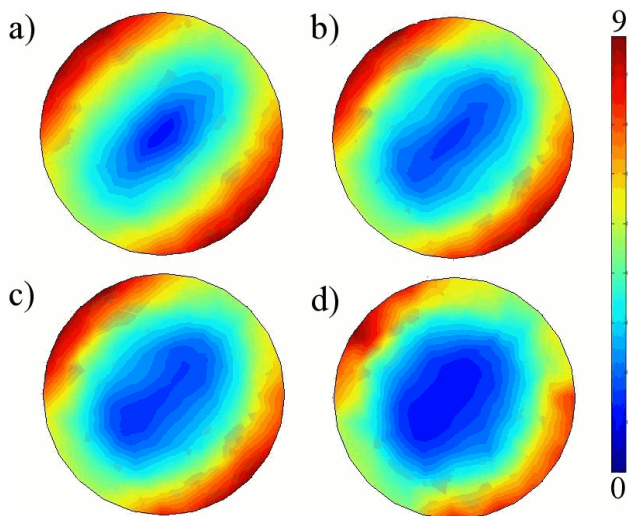


FIGURE 7. The RF field, B1, of our coil was numerically simulated for various resonant frequencies. The following frequencies were used: a) 64 MHz, b) 128 MHz, c) 171 MHz, and d) 256 MHz.

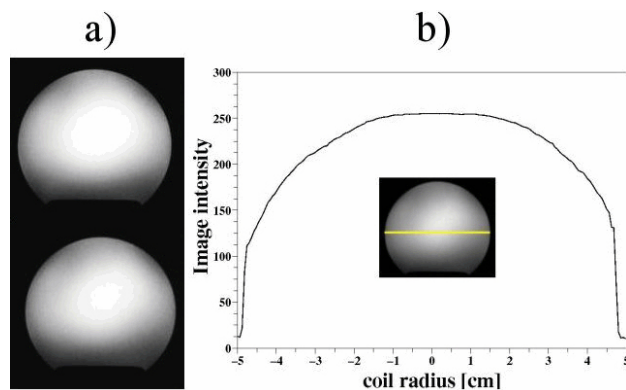


FIGURE 8. a) Phantom images in axial cuts acquired with our coil design and using standard spin-echo sequences and, b) A uniformity profile was computed from phantom image data along the yellow line shown in the image.

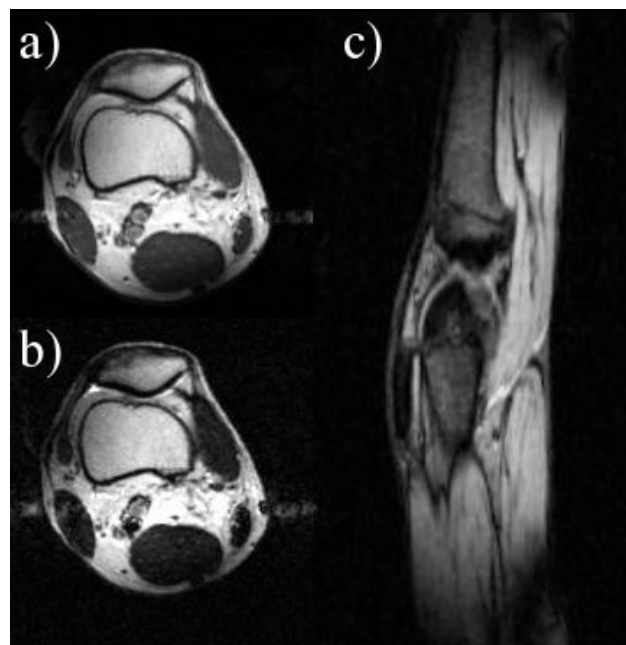


FIGURE 9. Transversal (a and b) and saggital (c) spin echo images of a normal knee in a male volunteer obtained with the birdcage coil. T1-weighted images show a high SNR and a good uniformity.

several possible pixel formats. The header file is represented here as a C structure which describes the dimensions and history of the pixel data. All images were digitally processed with the image processing software tool, Osirix Medical Imaging Software, v. 2.7.5 [14]. This software tool is dedicated to DICOM images produced by a medical system and has been particularly designed for the visualization of multimodalities and multidimensional images.

3. Results and discussion

The numerical simulations of the RF field were numerically computed and are shown in Figs. 6 and 7. Magnetic field simulations were performed: a) at different resonant frequencies

and b) varying the number of legs. In both cases simulations are in good agreement with results published in the literature [15], and show a fairly good B1-field uniformity despite the fact we used only four legs in our design [16]. Numerical simulations done by Jianming [15-16] showed that coils with a greater number of legs produce a more uniform B1-field than those with a lesser number of legs. However, our simulations do not show a clear improvement of the B1-field uniformity with the varying number of legs (Fig. 6). The resonant frequency has a minor effect on the B1-field uniformity for this birdcage resonator (Fig. 7), which is probably related to the low number of legs used in the coil design.

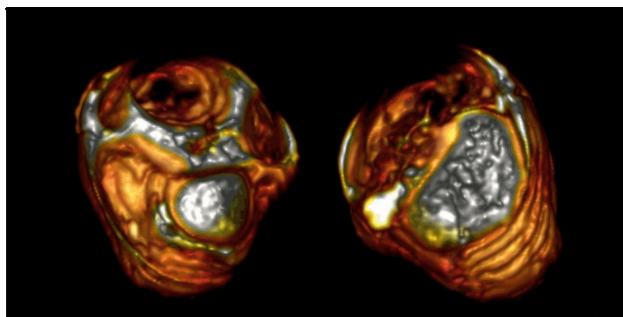


FIGURE 10. Three-dimensional reconstructions of knee images computed from transversal images of Fig. 9.

Phantom images were then acquired using standard spin-echo sequences and shown in Fig. 8a. The B1 uniformity profile of Fig. 8b was calculated from the spin-echo image of Fig. 8a, and it shows a fairly good agreement with the numerical simulations reported by Jianming and collaborators [16]. Finally, weighted-T1 and -T2 knee images of a healthy volunteer were also acquired in a different orientation with a standard spin-echo sequence. Fig. 9 shows T1-weighted images in axial and sagittal orientations.

The primary goal of this study was to test our first birdcage coil prototype by acquiring MR images of a phantom and a healthy knee at high field (4T) with conditions as similar as possible to those commonly found in daily clinical practice. Four studies were conducted with one healthy male

volunteer using standard spin-echo sequences and the birdcage resonator coil design. Examples of the *in vivo* knee images with the standard spin-echo sequence are presented in Fig. 9. With these images, a three-dimensional reconstruction of a knee was performed according to Sec. 2.5 and is shown in Fig. 10. Knee images compare very well with those reported elsewhere [17]. The spin-echo sequence was mainly used because of its widespread use in clinical practice in hospitals. Other pulse sequences such as gradient-echo sequences and the very popular parallel imaging technique promise a reduction in time without greatly sacrificing the SNR and are currently being studied. From these encouraging results, it can be also said that volume coils can be a good choice for imaging the knee, mainly because of its good uniformity and higher SNR when combined with high field MRI imagers.

This preliminary experience with a 4T MR imager and the birdcage coil together with standard pulse sequences is a feasible and reliable method for acquisition of high-spatial resolution MR images of the healthy knee. For this type of assessment further clinical studies including healthy volunteers and patients with knee abnormalities should be involved. There is a growing interest to investigate whether the higher SNR produced by high field MR imagers (>1.5 Tesla) is able to improve the study of pathologies of the knee [18].

In conclusion, our theoretical simulations and experimental results suggests that a four-leg birdcage has an acceptable SNR and B1-field uniformity for imaging human knees at high magnetic field strength (4-Tesla).

Acknowledgments

S. E. S. wishes to thank the National Council of Science and Technology of Mexico (CONACyT) for a Ph. D. scholarship, and grant numbers: 53107, 1-35119 and 1-35106, and Laboratory Directed Research and Development from U.S. Department of Energy (OBER). Support from Innovamedica is gratefully appreciated.

*. Corresponding author: e-mail: arog@xanum.uam.mx

1. C.E.Hayes, W.A. Edelstein, J.F. Schenck, and O.M. Mueller, *J. Magn. Reson.* **63** (1985) 622.
2. C.N. Chen, D.I. Hoult, and V.J. Sank, *J. Magn. Reson.* **54** (1983) 324.
3. R.J. Pascone, T. Vullo, J. Farrell, R. Mancuso, P.T. Cahill, *Magn. Reson. Imaging.* **11** (1993) 705.
4. F.D. Doty, G. Entzminger G., C.D. Hauck, and J.P. Staab, *J. Magn. Reson.* **138** (1999) 144.
6. R.J. Pascone *et al.*, *Magn. Reson. Imaging.* **9** (1991) 395.
5. T. Vullo, R.T. Zipagan, R.J. Pascone, J.P. Whalen, P.T. Cahill, *Magn. Reson. Med.* **24** (1992) 243.

6. G. Giovannetti, L. Landini, and M.F. Santarelli, *MAGMA* **15** (2002) 36.
7. C.L. Chin, C.M. Collins, S. Li, B.J. Dardzinski, and M.B. Smith, *Conc. Magn. Reson. Part B: Magn. Reson. Engineering.* **15** (2002) 156.
8. C.M. Collins, S. Li, Q.X. Yang, and M.B. Smith, *J. Mag. Reson.* **125** (1997) 233.
9. M.D. Harpen, *Magn. Reson. Med.* **29** (1993) 263.
10. W. Schnell, W. Renz, M. Vester, and H. Ermert, *IEEE Trans. Ant. Prop.* **48** (2000) 418.
11. Y. Xu and P. Tang, *Magn. Reson. Med.* **38** (1997) 168.
12. J.C. Watkins and E. Fukushima, *Rev. Sci. Instrum.* **59** (1988) 926.

13. ANALYZE^a software. URL: www.mayo.edu/bir/software/Analyze/Analyze1.html
14. Osirix medical imaging software. URL: www.osirix-viewer.com
15. J. Jianming, *Electromagnetic analysis and design* (CRC Press: Boca Raton 1998).
16. J. Jianming, G. Shen, and T. Perkins, *Magn. Reson. Med.* **32** (1994) 418.
17. E.H.G. Oei, A.Z. Ginai, and M.G.M. Hunink, *Sem. US CT MRI.* **28** (2007) 141.
18. P.M. Cunningham, M. Law, and M.E. Schweitzer, *Orthop. Clin. North. Am.* **37** (2006) 321.